An elastic plate model for wave attenuation and ice floe breaking in the marginal ice zone

A. L. Kohout[1] and M. H. Meylan[1]

Received 4 July 2007; revised 4 February 2008; accepted 2 June 2008; published 9 September 2008.

[1] We present a model for wave attenuation in the marginal ice zone (MIZ) based on a two-dimensional (one horizontal and one vertical dimension) multiple floating elastic plate solution in the frequency domain, which is solved exactly using a matched eigenfunction expansion. The only physical parameters that enter the model are length, mass, and elastic stiffness (of which, the latter two depend primarily on thickness) of the ice floes. The model neglects all nonlinear effects as well as floe collisions or ice creep and is therefore most applicable to floes which are large compared to the thickness and to wave conditions which are not extreme. The solution for a given arrangement of floes is fully coherent, and the results are therefore dependent on the exact geometry. We firstly show that this dependence can be removed by averaging over a distribution of floe lengths (we choose the Rayleigh distribution). We then show that after this averaging, the attenuation coefficient is a function of floe number and independent of floe length, provided the floe lengths are sufficiently large. The model predicts an exponential decay of energy, just as is shown experimentally. This enables us to provide explicit values for the attenuation coefficient, as a function of the average floe thickness and wave period. We compare our theoretical predictions of the wave attenuation with measured data and other scattering models. The limited data allows us to conclude that our model is applicable to large floes for short to medium wave periods (6 to 15 seconds). We also derive a floe breaking model, based on our wave attenuation model, which indicates that we are under-predicting the attenuation coefficients at long periods.

Citation: Kohout, A. L., and M. H. Meylan (2008), An elastic plate model for wave attenuation and ice floe breaking in the marginal ice zone, *J. Geophys. Res.*, *113*, C09016, doi:10.1029/2007JC004434.

1. Introduction

[2] The sea-ice which forms in the polar oceans plays an important role in the world's climatic system. It is therefore important to understand the processes which influence the extent of this sea-ice. *Squire et al.* [1995] and *Wadhams* [2000] have evidence suggesting that ocean waves play a major role in the fracturing of ice-covered seas. The analysis of this phenomenon involves many complicated variables, and considerable idealization is required. One aspect which is critical to understand is the attenuation of wave energy as it passes through the marginal ice zone (MIZ).

[3] The MIZ is an interfacial region which forms at the boundary of open and frozen oceans. It consists of a vast field of ice floes, and it is subject to considerable wave action due to its proximity to the open ocean. A number of experiments measuring wave propagation through the MIZ have been reported. The first measurements of wave decay through ice floes were made by a ship-borne wave recorder [*Robin*, 1963; *Dean*, 1966]. Later measurements were made by upward-looking echo sounder from a submerged hovering submarine [*Wadhams*, 1978] and by airborne laser profilometer [*Wadhams*, 1975]. An important series of experiments were carried out by the Scott Polar Research Institute (SPRI) and they allowed the wave attenuation coefficients to be calculated [*Squire and Moore*, 1980; *Squire et al.*, 1983; *Wadhams et al.*, 1988]. Another set of field experiments were from the Labrador Ice Margin Experiment (LIMEX), which were carried out in March 1987, off the east coast of Newfoundland, Canada [*Liu et al.*, 1991]. These experiments provided aircraft synthetic aperture radar (SAR), wave buoy and ice property data. Most recently, some successful measurements have been made off the West Antarctic Peninsula, where an upward-looking Acoustic Doppler Current Profiler (ADCP) was mounted on an autonomous underwater vehicle (AUV). Throughout all of these experiments, it has been shown that wave energy decays exponentially with distance of propagation into a MIZ, and that this rate of decay is highly dependent on the wave period and floe thickness.

[4] A number of models for wave propagation in the MIZ have been presented. In general they can be divided into models based on wave scattering by individual ice floes and models based on other physics or parameters, such as the models derived from the eddy viscosity [*Liu et al.*, 1991] or using the coherent potential approximation [*Dixon and Squire*, 2001]. We will describe the wave

[1]Department of Mathematics, University of Auckland, Auckland, New Zealand.

0148-0227/08/2007JC004434

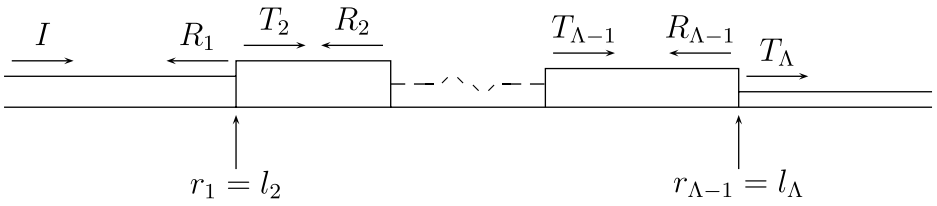

Figure 1. A schematic diagram showing the set of ice floes and the coordinate systems used in the solution. The two-dimensional region is defined by $-\infty < x < \infty$ and $-h < z \leq 0$, where we assume constant depth h. I is the incident wave. R_μ and T_μ are the reflection and transmission coefficients of the μth plate. l_μ and r_μ are the left and right edges of the floe μ. There are Λ floes, where the first and last are semi-infinite. Note that the first plate represents the open ocean.

scattering models in detail here. An elastic plate model is described in *Wadhams* [1986] where the possible paths of each wave vector through the ice field are considered and the final forward vector summed through multiple reflections. However the correct solution for a single two-dimensional floe was not found until the work of *Meylan and Squire* [1994]. The most sophisticated models developed were fully three-dimensional models which coupled the solutions for individual ice floes with a transport equation [*Masson and LeBlond*, 1989; *Meylan et al.*, 1997]. (Note that [*Masson and LeBlond*, 1989] did not model the floe as an elastic plate, but such a formulation could easily be incorporated into their model). These three-dimensional models, which were derived separately, have been recently shown to be almost identical [*Meylan and Masson*, 2006]. Unfortunately, significant work is required for the models of [*Masson and LeBlond*, 1989; *Meylan et al.*, 1997] to reach the point where predictions of the attenuation coefficients are possible and such predictions require large computational resources, so that no summary of attenuation coefficient as a function of various parameters has been possible. *Perrie and Hu* [1996] used the scattering model of [*Masson and LeBlond*, 1989] in an operational wave model, and they predicted the attenuation coefficients. However they used a rigid floe model which is only applicable to small floes.

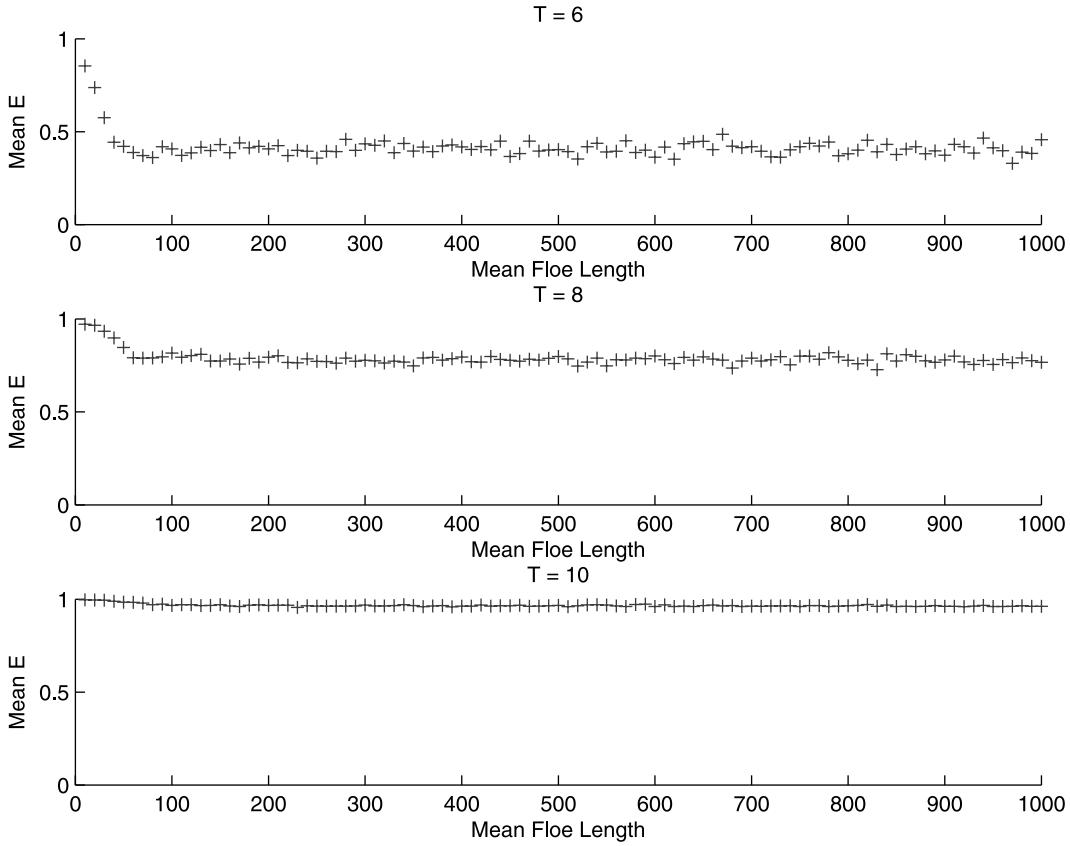

Figure 2. The normalized mean transmitted energy, E versus mean floe length (m), where the floe lengths are chosen via a Rayleigh distribution about the mean. For each mean floe length, E is averaged over 100 simulations. For each subplot τ is distributed, with a standard deviation of 0.05, about 1 m, $\Lambda = 10$ and T (s) varies as indicated.

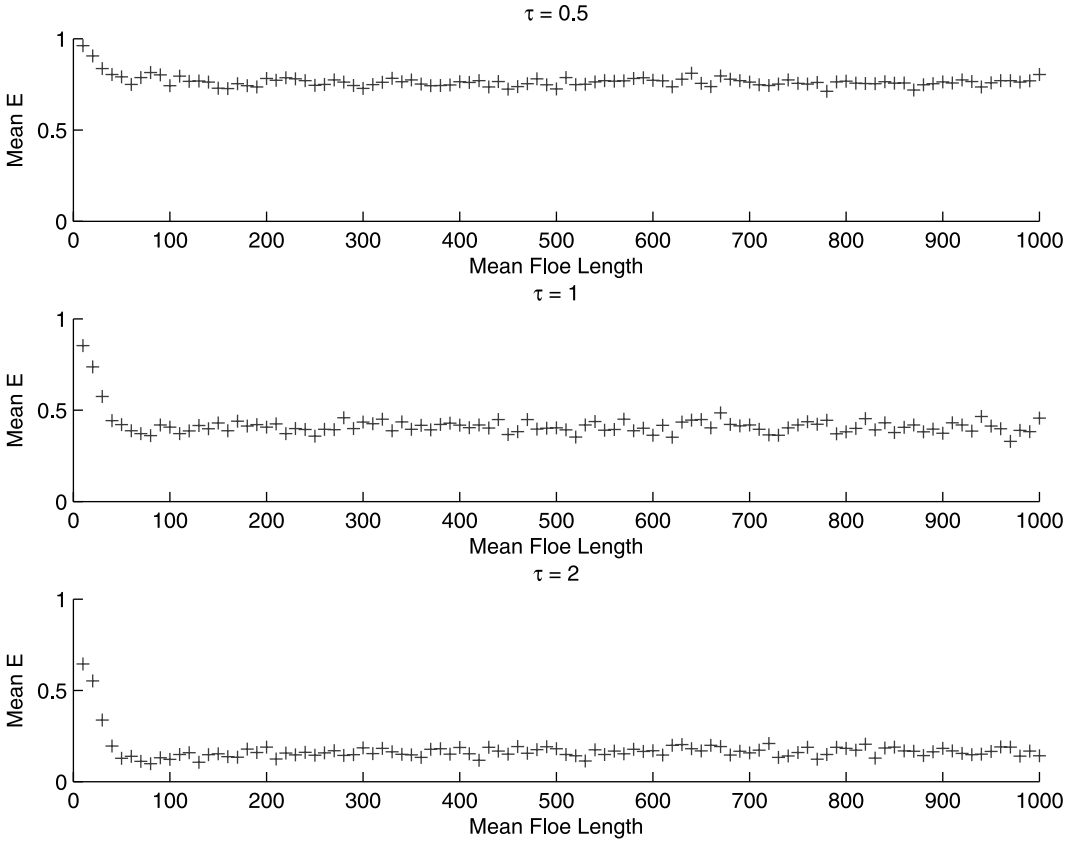

Figure 3. The normalized mean transmitted energy, E versus mean floe length, where the floe lengths are chosen via a Rayleigh distribution about the mean. For each mean floe length, E is averaged over 100 simulations. For each subplot $\Lambda = 10$, $T = 6$ s, and τ (m) is distributed, with a standard deviation of 0.05, about a mean as indicated.

[5] The present model is based on the elastic bending of the floes and does not allow for any other physics. This limits the range of applicability of the model, but it also means that we can determine numerical values for the attenuation coefficient straightforwardly. Furthermore, by comparing our results with measured data we can determine for which conditions the elastic plate model will be appropriate. It is also worth noting, that the elastic plate model reduces to the rigid floe model when the floe length becomes small.

[6] The outline of the paper is as follows. In section 2 we explain our two-dimensional solution for multiple floating plates based on an eigenfunction expansion, which we solve by matching these expansions at each plate boundary. This section is only a summary. The full details of the solution method can be found in *Kohout et al.* [2007]. In section 3, our solution is used to simulate an idealized MIZ. Here we establish that the attenuation coefficient is independent of floe length, provided that the average floe length is sufficiently large and that the wave energy, without making any priori assumptions, decays exponentially with distance into the MIZ. We calculate values for the attenuation coefficients as a function of period and thickness. In section 4, we describe a series of field experiments [*Wadhams et al.*, 1988; *Hayes et al.*, 2007], which measured wave attenuation in the MIZ. In section 5 we compare our model to these experiments and in section 6 we use our model to predict floe breaking. Section 7 is a summary. A preliminary version of this model was published in *Kohout and Meylan* [2006], which focused only on coherence and displacement, and did not present any averaged results or comparison with data and other models.

2. The Two-Dimensional Model for Wave-Ice Interaction

[7] We present here the outline of our model for wave-ice interactions based on a solution for a finite number of floating elastic plates. It is worth stating from the outset that the only physics in this model are due to the interaction of the waves with an elastic boundary layer at the surface of the water. We are neglecting all other effects such as viscosity, floe collisions, and nonlinear effects. We also consider only small-amplitude waves. In the formulation presented here, we assume that the set of floating elastic plates occupies the entire water surface. We can simulate open water by a very thin plate, or by a separate formulation. Numerically there is no difference, and the separate formulation is not presented here. The problem is two-dimensional, and the solution is based on a matched eigenfunction expansion. The solution is described in detail in *Kohout et al.* [2007], where the results are carefully analyzed for energy conservation,

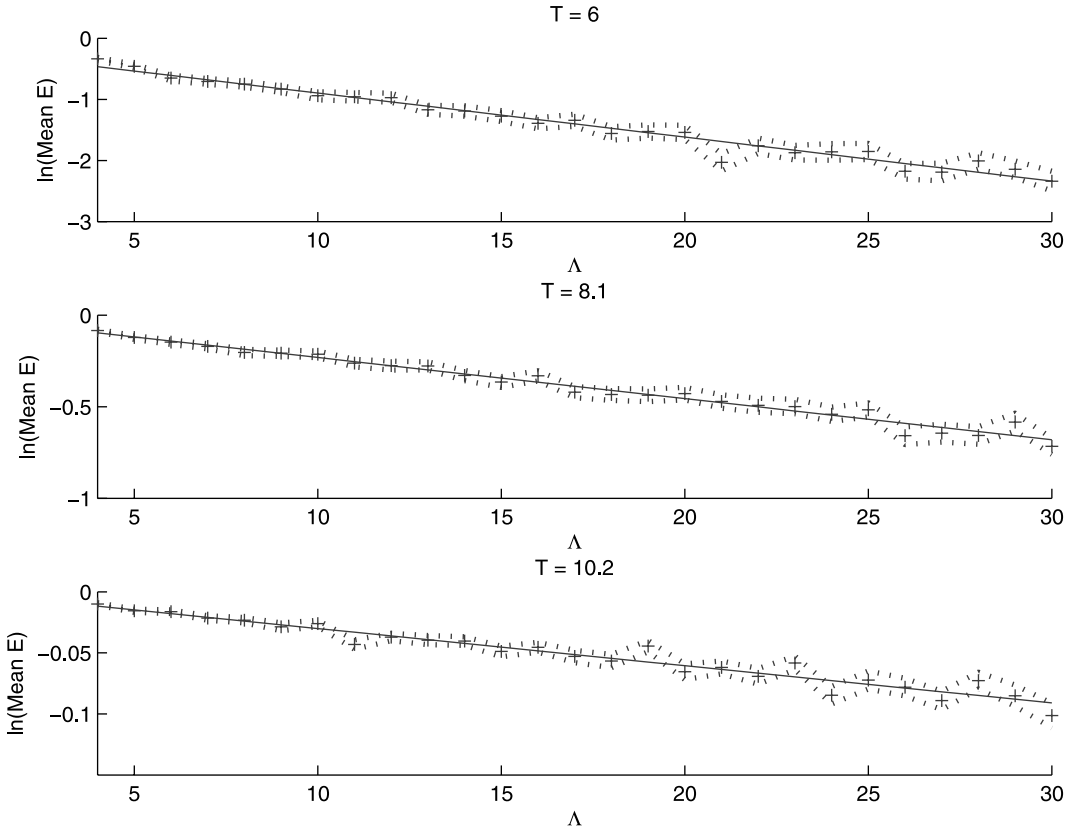

Figure 4. Mean ln(E) versus Λ. For each Λ, E is averaged over 100 trials and the dotted line gives the 67% confidence interval for E (one standard deviation). τ is distributed, with a standard deviation of 0.05, about a mean of 1 m and T (s) varies for each subplot as indicated. The solid line shows a straight line fit to the data.

compared against other models, and with a series of experiments that were performed by *Sakai and Hanai* [2002] using floating plastic sheets in a two-dimensional wave tank. We are therefore confident of the validity of the numerical solution which underlies our model. In *Kohout et al.* [2007] we also show how we can solve for waves incident at an angle. This effect is discussed in [*Wadhams et al.*, 1986] but we do not consider it here.

[8] In our problem, the submergence of the plates is considered negligible. We assume that the problem is invariant in the y direction and, for simplicity, allows the waves to be normally incident. The set of plates consists of two semi-infinite plates, separated by a region which consists of a finite number of plates with variable properties. We simulate open water by setting the plate properties, i.e., thickness, to be small (rather than by introducing an additional formulation). We assume that the plate edges are free to move at each boundary. A schematic diagram of the problem is shown in Figure 1.

[9] The standard mathematical description of the problem is as follows. Throughout the fluid Laplace's equation holds,

$$\nabla^2\phi = 0 \qquad \text{for} \quad -h < z \leq 0, \tag{1}$$

at the seabed with a constant depth, h, there is no flow,

$$\frac{\partial\phi}{\partial z} = 0 \qquad \text{at} \quad z = -h, \tag{2}$$

and at the surface the nondimensional plate equation holds,

$$\left(\beta_\mu \frac{\partial^4}{\partial x^4} - \gamma_\mu\alpha + 1\right)\frac{\partial\phi}{\partial z} - \alpha\phi = 0 \qquad \text{at} \quad z = 0, \qquad l_\mu \leq x \leq r_\mu, \tag{3}$$

where $\alpha = (2\pi/T)^2$ with period T, $\beta_\mu = D_\mu/\rho_\mu g L^4$ is the stiffness constant of the μth plate where ρ_μ is the mass density of the μth plate, and $D_\mu = Y\tau_\mu^3/12(1-\nu^2)$ is the rigidity constant where Y is the Young's modulus, τ_μ is the thickness of the μth plate, and ν is Poison's ratio; $\gamma_\mu = m_\mu/\rho L$ is the mass constant of the μth plate where ρ is the water density and $m_\mu = \rho_\mu\tau_\mu$; and l_μ and r_μ are the left and right edges of the floe μ. At the plate edges, the free-edge conditions apply

$$\frac{\partial^3}{\partial x^3}\frac{\partial\phi}{\partial z} = 0 \qquad \text{at } z = 0 \qquad \text{for } x = l_\mu, r_\mu, \tag{4}$$

$$\frac{\partial^2}{\partial x^2}\frac{\partial\phi}{\partial z} = 0 \qquad \text{at } z = 0 \qquad \text{for } x = l_\mu, r_\mu. \tag{5}$$

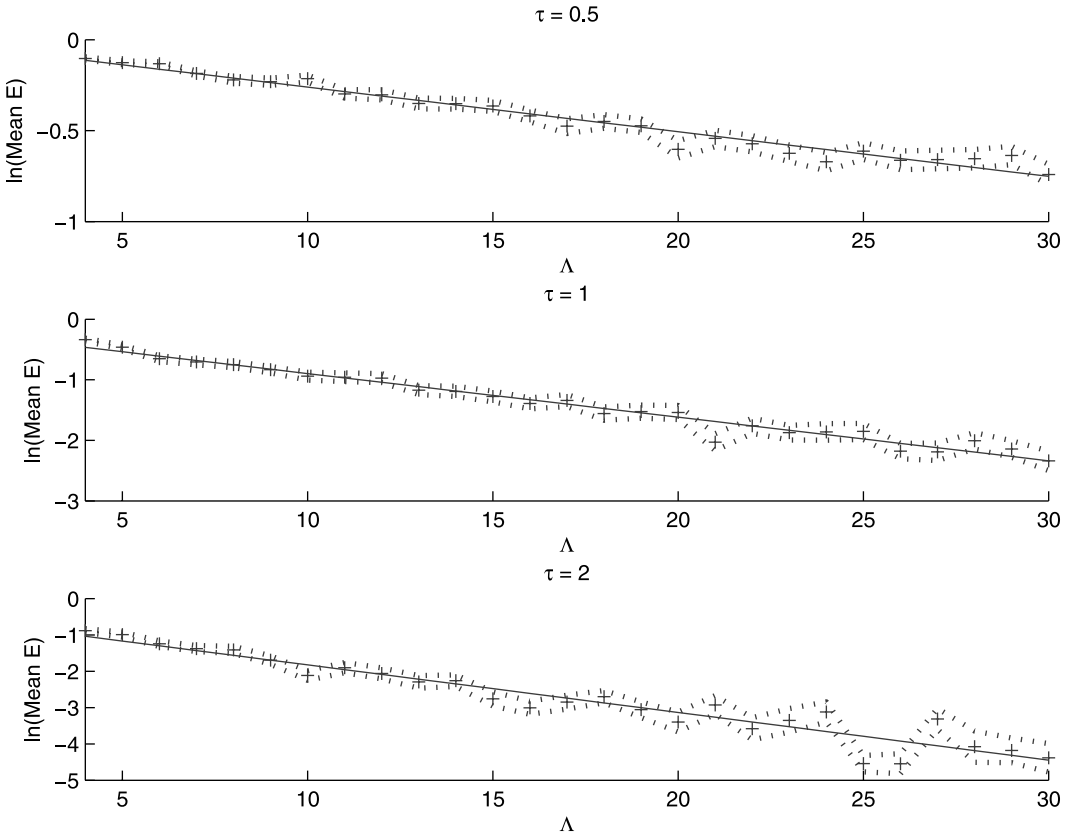

Figure 5. Mean ln(E) versus Λ. For each Λ, E is averaged over 100 trials and the dotted line gives the 67% confidence interval for E (one standard deviation). $T = 6$ s and τ (m) is distributed, with a standard deviation of 0.05, about the mean as indicated for each subplot. The solid line shows a straight line fit to the data.

[10] Note that the assumptions and formulations up to this point are identical to those given in *Wadhams* [1986]. We solve equations (1) to (5) using an eigenfunction expansion. This method has been applied in many situations for linear water wave problems, and the technique is described in *Linton and McIver* [2001]. Our method extends the solution given in *Fox and Squire* [1994] from a single ice–water interface to multiple plates, and it also presents a simpler method to derive the coefficients based on an inner product rather than error minimization. The first and last plates are semi-infinite and the middle plates are finite. The potential velocity of the first plate can be expressed as the summation of an incident wave and of reflected waves, one of which is traveling, two of which are damped traveling, and the rest of which are evanescent and decay as x tends to $-\infty$. Similarly the potential under the final plate can be expressed as a sum of transmitting waves, one of which is traveling, two of which are damped traveling, and the rest of which are evanescent and decay toward $+\infty$. The potential under the middle plates can be expressed as the sum of transmitting waves and reflected waves, each of which consists of a traveling, two damped traveling, and evanescent waves which decay as x increases or decreases, respectively. We could combine these waves in the formulation, but due to the exponential growth (or decay) in the x direction the solution becomes numerically unstable in some cases if the transmission and reflection are not expanded at opposite ends of the plate.

[11] The potential velocity, under each elastic plate, can be written in terms of an infinite series of eigenfunctions of the form

$$\phi = e^{k_\mu x}\cos\big(k_\mu(z+h)\big). \tag{6}$$

If we apply the boundary conditions given by equations (2) and (3), we obtain

$$k_\mu \tan\big(k_\mu h\big) = -\frac{\alpha}{\beta_\mu k_\mu^4 + 1 - \alpha\gamma_\mu}. \tag{7}$$

Solving for k_μ, this dispersion equation (7) gives a pure imaginary root with positive imaginary part, two complex conjugate roots, an infinite number of positive real roots which approach $n\pi/h$ as n approaches infinity, and also the negative of all these roots [*Fox and Squire*, 1994]. We denote the two complex roots with positive imaginary part by $k_\mu(-2)$ and $k_\mu(-1)$, the purely imaginary root with positive imaginary part by $k_\mu(0)$ and the real roots with positive imaginary part by $k_\mu(n)$ for n a positive integer. The imaginary roots correspond to two traveling modes traveling along the x axis. The complex roots correspond to damped traveling modes and the real roots correspond to the evanescent modes.

[12] We now expand the potential under each plate. We always include the two complex and one imaginary root, and truncate the expansion at M real roots of the dispersion equation.

[13] The potential ϕ can now be expressed as the following sum of eigenfunctions:

$$\phi \approx \begin{cases} Ie^{k_1(0)(x-r_1)}\dfrac{\cos(k_1(0)(z+h))}{\cos(k_1(0)h)} \\ \quad + \displaystyle\sum_{n=-2}^{M} R_1(n)e^{k_1(n)(x-r_1)}\dfrac{\cos(k_1(n)(z+h))}{\cos(k_1(n)h)}, \\ \qquad \text{for } x < r_1, \\ \displaystyle\sum_{n=-2}^{M} T_\mu(n)e^{-k_\mu(n)(x-l_\mu)}\dfrac{\cos(k_\mu(n)(z+h))}{\cos(k_\mu(n)h)} \\ \quad + \displaystyle\sum_{n=-2}^{M} R_\mu(n)e^{k_\mu(n)(x-r_\mu)}\dfrac{\cos(k_\mu(n)(z+h))}{\cos(k_\mu(n)h)}, \\ \qquad \text{for } l_\mu < x < r_\mu, \\ \displaystyle\sum_{n=-2}^{M} T_\Lambda(n)e^{-k_\Lambda(n)(x-l_\Lambda)}\dfrac{\cos(k_\Lambda(n)(z+h))}{\cos(k_\Lambda(n)h)}, \\ \qquad \text{for } l_\Lambda < x, \end{cases} \tag{8}$$

where I is the incident wave amplitude, μ is the μth plate, Λ is the last plate, r_μ is the x-coordinate of the right edge of the μth plate, l_μ is the x-coordinate of the left edge of the μth plate, $R_\mu(n)$ is the reflected potential coefficient of the nth mode under the μth plate, and $T_\mu(n)$ is the transmitted potential coefficient of the nth mode under the μth plate.

[14] We solve for the coefficients in the expansion by matching the potential and its x derivative at each plate boundary and by applying the boundary conditions at each plate boundary. To solve for the coefficients, we require as many equations as we have unknowns. We derive the equations from the free-edge conditions and by imposing conditions of continuity of the potential and its derivative in the x-direction at each plate boundary. We impose the latter condition by taking inner products with respect to the orthogonal functions $\cos\frac{m\pi}{h}(z+h)$, where m is a natural number. These functions were chosen due to their simplicity and because in the limit of large n the vertical eigenfunctions under the plate approach these functions. Taking inner products leads to the following equations

$$\int_{-h}^{0}\phi_\mu(r_\mu,z)\cos\frac{m\pi}{h}(z+h)dz = \int_{-h}^{0}\phi_{\mu+1}(l_{\mu+1},z)\cos\frac{m\pi}{h}(z+h)dz, \tag{9}$$

$$\int_{-h}^{0}\frac{\partial\phi_\mu}{\partial x}(r_\mu,z)\cos\frac{m\pi}{h}(z+h)dz = \int_{-h}^{0}\frac{\partial\phi_{\mu+1}}{\partial x}(l_{\mu+1},z)\cos\frac{m\pi}{h}(z+h)dz, \tag{10}$$

where $m \in [0, M]$ and ϕ_μ denotes the potential under the μth plate, i.e., the expression for ϕ given by equation (8) valid for $l_\mu < x < r_\mu$. The remaining equations to be solved are given by the free-edge conditions (4) and (5).

3. Simulating Wave Propagation in the MIZ

[15] An approximation for the attenuation coefficient, based on a solution for a single two-dimensional finite floe surrounded by water, is given in *Wadhams* [1986], based on a multiple scattering approximation. The approximation is given by

$$a \approx -\frac{1}{2}\ln\left(\frac{|T_3|^2}{2-|T_3|^2}\right), \tag{11}$$

where T_3 is the transmission coefficient for a single floe. An even simpler approximation can be found by assuming only a single scattering and we obtain

$$a \approx -\ln\left(|T_3|^2\right), \tag{12}$$

and this is given in *Wadhams et al.* [1988]. Note that these two approximations become equal in the limit of small T_3. Unfortunately, no numerical method to solve the problem of a single floe had been developed at that time, and the solutions in *Wadhams et al.* [1986, 1988] used only a subset of the evanescent modes. In Appendix A we derive a formula for the average T_3 assuming the floe is sufficiently long, and this is used for the value of T_3 in the approximations for a given by equations (11) and (12) in subsequent comparisons.

[16] A MIZ wave attenuation model is also developed by *Perrie and Hu* [1996], which is based on *Masson and LeBlond* [1989] and uses a rigid cylindrical floe model [*Isaacson*, 1982]. The scattering model is incorporated into an operational wave model. The model suffers from the requirement that the ice floes be small enough to be modelled as rigid cylinders, so that it is only applicable to small floes. It would be interesting to see how the model performed with a more sophisticated three-dimensional ice floe model, such as the elastic plate model of *Meylan* [2002].

[17] We now describe how our model is used to simulate an ocean wave propagating under a set of ice floes. The number of evanescent modes required depends on the water depth. We set the water depth sufficiently large so that it can be considered infinite (in practice this depth is one wavelength, i.e., the nondimensional depth is $h = 2\pi/k$). We set $N = 20$ as we find that this gives a good compromise of accuracy and computational time. It is worth noting that the long period waves, for which it is more difficult to determine the attenuation coefficients, require fewer modes to get good convergence. We choose the following values for the constants: $Y = 6$ GPa, $\nu = 0.3$, $g = 9.8$ ms^{-2}, $\rho = 1025.0$ kgm^{-3}, and $\rho_\mu = 922.5$ kgm^{-3}. It is important to recognize that, because we have assumed the ice floes are thin, the nondimensional stiffness β_μ is much more significant than the nondimensional mass γ_μ. This means that the effect of changing the Young's modulus is equivalent to changing the cube root of the thickness. For this reason we will not consider any other values for Y. In all results the semi-infinite plate on the left is open water. The semi-

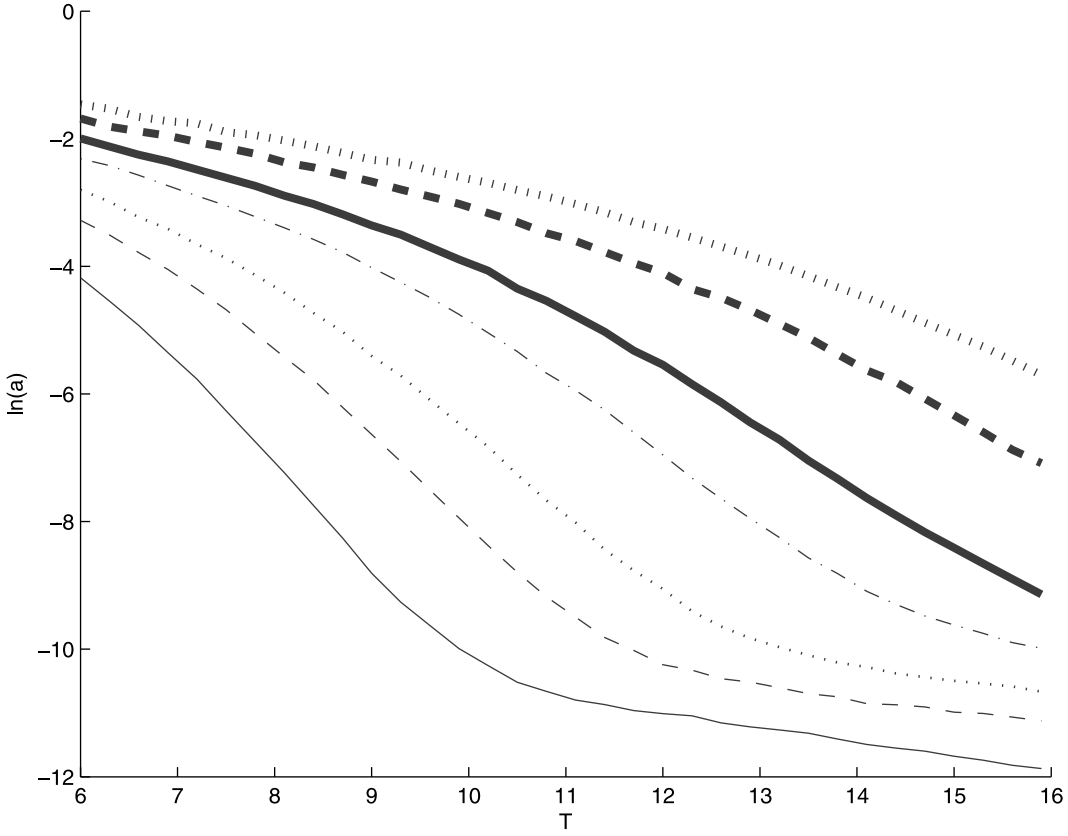

Figure 6. Predictions of the logarithm of the attenuation coefficient, ln(a), versus T (s) for τ = 0.4 m (−), τ = 0.6 m (− −), τ = 0.8 m (· · ·), τ = 1.2 m (− · −), τ = 1.6 m (−), τ = 2.4 m (− −), and τ = 3.2 m (· · ·).

infinite plate to the right is a semi-infinite ice floe which is chosen to have the same thickness as the other floes (if the floe thicknesses are different and chosen randomly then the thickness of the semi-infinite floe is also random). A wave is incident from the left-hand (open water side) with unit amplitude, and the transmitted energy in the right-hand semi-infinite plate can be calculated as $E = |1 - R_1|^2$ (this expression being a result of the condition that the incident energy is equal to the sum of the radiated energy). To simulate the MIZ, we have also added gaps of water between each floe, and the thickness τ of each floe is chosen normally about a mean. In our simulation, we have a number of variables; the incident period (s), T; the length of each floe (m), L (which can differ per floe); the thickness of each floe (m), τ (which can differ per floe); and the number of floes, Λ (note that the number of finite floes is $\Lambda - 2$).

3.1. Simulation

[18] One of the critical features of the model (and all models which use linear wave theory) is that it is fully coherent. This means that we will always observe effects of cancellation and addition of waves, no matter how large the ice floes size or number of ice floes. The effect of this coherence is discussed in detail in *Kohout and Meylan* [2006]. One of the most important ideas which underlies this model is the idea of simulating and averaging to remove these coherent effects. This method has also been considered in *Wadhams* [1986] and *Williams and Squire* [2004, 2006]. To remove this resonance, we allow the floe length to vary for each floe about a fixed mean, and we average over many trials. We assume that the spread of floe lengths in the MIZ fits a Rayleigh distribution. We select each floe length to follow a Rayleigh distribution about a given mean and we also include Rayleigh distributed gaps between floes (we have tried other distributions and the results are nearly identical). All the results we will present will be the average of 100 simulations.

3.2. Floe Length

[19] The first result from our simulations is that the average of E is independent of length, provided that the floe length is above a critical value. This is shown in Figures 2 and 3, where we consider the effect of the parameters T and τ. These figures show that the critical length above which E is independent of mean floe length depends strongly on T and slightly on τ. The physical explanation for this effect is as follows. If the floe is sufficiently long it must bend in response to the waves. This bending induces reflections at the edges, but allows the waves to propagate under the floes without attenuation (since our ice floe is modelled as perfectly elastic). This means that the attenuation can be expected to depend only on the number of interfaces, with obvious analogy to other wave scattering processes. However, once the floe length becomes sufficiently short so that the floe is no longer required to bend, there is no longer any notion of a

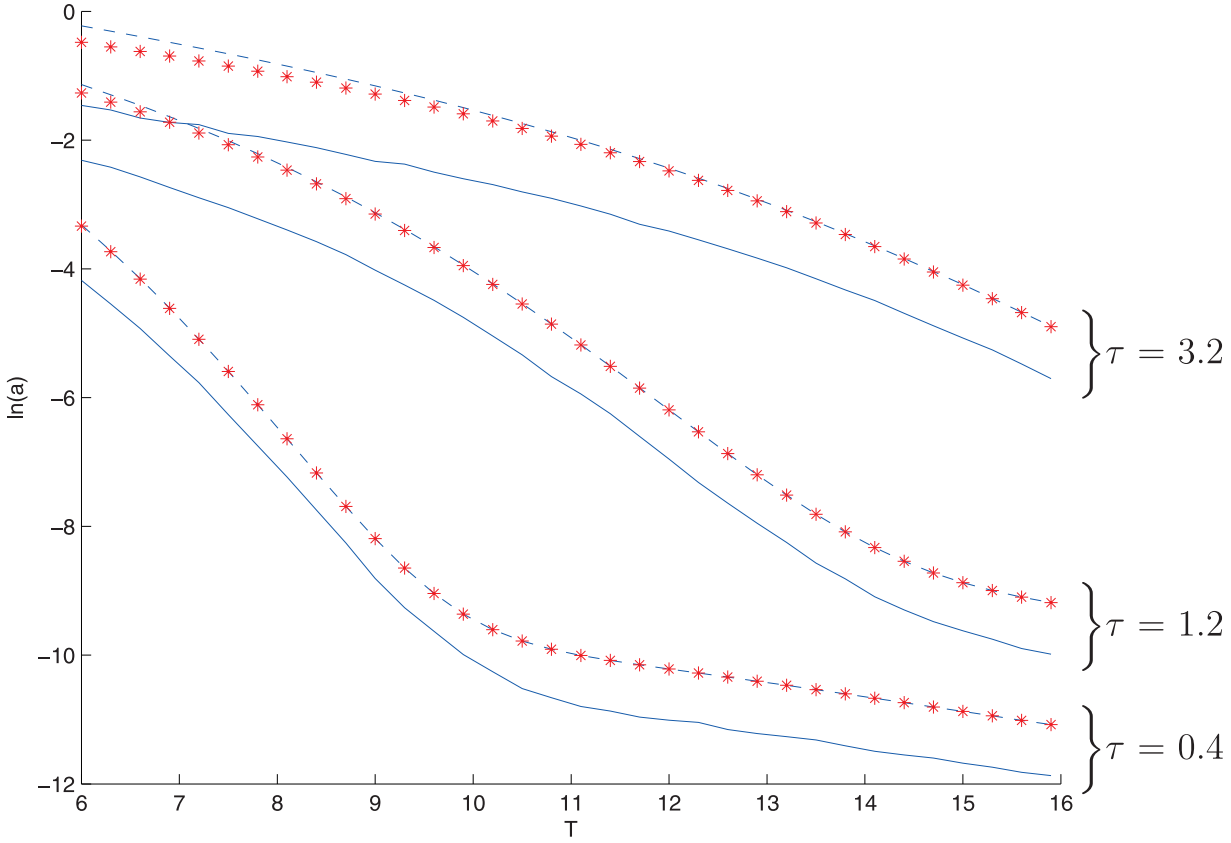

Figure 7. A comparison between the attenuation coefficients from our model (-) versus the attenuation coefficients from Wadhams' approximation theories, for $\tau = 0.4$, 1.2, and 3.2 m. The data points (*) give the attenuation coefficients from (11) and the dashed lines (- -) give the attenuation coefficients from (12). T_3 in equations (11) and (12) is given by T_{av} which is derived in Appendix A.

wave propagating under the floe. Furthermore, as the floe shortens it will reflect less energy. It can be expected that this critical length will occur roughly when the wavelength is more than two or three times the floe length. We generally restrict our model to the large floe length case, but we can simulate shorter floe lengths with our model and will do so if appropriate.

3.3. Effect of the Number of Floes

[20] The value of transmitted energy E depends strongly on the number of floes Λ, and we find that this dependence is exponential. Figures 4 and 5 show the fit of E to an exponential curve and show that our model is predicting exponential decay of energy just as is measured. We will now concentrate our results on the exponential attenuation coefficient, which is precisely what is measured experimentally.

3.4. Attenuation Coefficient

[21] We assume that the energy E decays exponentially with number of floes, Λ, i.e.

$$E \propto e^{-a\Lambda} \tag{13}$$

where a is the attenuation coefficient and E is normalized with unit incidence. From Figures 4 and 5, we can see that the attenuation coefficient, a, is dependent on both T and τ. Note that our definition of attenuation coefficient is different from the standard definition because it is normally assumed that the decay is proportional to distance. We will use α for the attenuation coefficient which is proportional to distance. Figure 6 gives $\ln(a)$ against T for various τ. This figure is the cornerstone of our results. The model provides a tool for predicting wave attenuation in the MIZ as well as comparing attenuation coefficients against other, perhaps more sophisticated, models and field experiments. The figure shows that the attenuation coefficient depends strongly on both wave period, T, and thickness, τ. The attenuation coefficient for fixed period, T, depends strongly on thickness, τ, and the attenuation coefficient for fixed thickness, τ, depends strongly on period, T. This figure explains why the MIZ acts

Table 1. Comparison of Greenland Sea Experimental Attenuation Coefficients From the 10th of September 1979 (α) Obtained From *Wadhams et al.* [1988], the Scaled Attenuation Coefficients ($\alpha \times 80/.17$) Against the Model Attenuation Coefficients (a)[a]

T s	α ($m^{-1} \times 10^{-4}$)	$\alpha \times 80/0.17$	a
6.73	2.01 ± 1.46	0.095 ± 0.069	0.196
7.37	2.37 ± 1.46	0.112 ± 0.069	0.134
8.14	2.35 ± 0.54	0.111 ± 0.025	0.115
9.10	1.29 ± 0.13	0.061 ± 0.006	0.094
10.31	1.25 ± 0.28	0.059 ± 0.013	0.059
11.88	0.89 ± 0.46	0.042 ± 0.022	0.028

[a]The ± values given represent the margin of error provided in *Wadhams et al.* [1988].

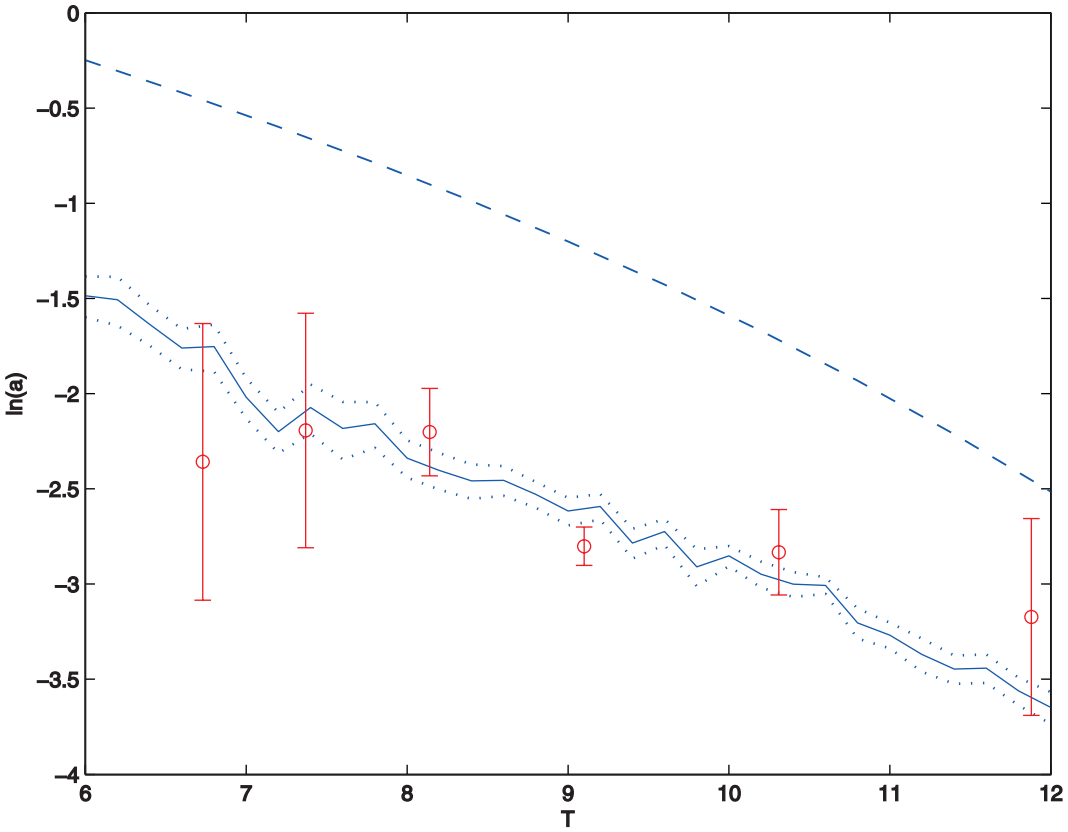

Figure 8. The attenuation coefficients for our model (solid line) and its 95% confidence interval (dotted lines), for the *Wadhams et al.* [1988]'s attenuation theory given by equation (12), where T_3 is given by T_{av} (dashed line), and for the Greenland Sea experiment on 10 September 1979 (o) against T. Error bars are included on the experimental data points.

so strongly as a low-pass filter (in the sense of frequency) and how important the parameter of thickness, τ, is in determining the properties of this filtering.

[22] Figure 7 shows a comparison between the attenuation coefficient from our model and the attenuation coefficient from the approximations given by (equations (11) and (12)). The approximate theories show exactly the same trends as the full scattering theory. They agree particularly well for thin plates. The reason why the scattering coefficient is lower for our model is because our model allows for all scattering (and conserves energy) and both models are based on a long floe length assumption.

4. Comparison With Data

[23] Theory and experiment need to work together to understand complicated geophysical phenomena such as wave-ice interactions. It is important to realize that the present situation is one where there has been much more progress with modeling than with experiments in recent years. The best data sets are nearly 30 years old. This is highly unsatisfactory, and from a modeler's perspective we have great need for more and better experimental results.

4.1. Description of Field Experiments

[24] The most important set of experiments to measure wave attenuation in the MIZ were carried out by the SPRI in the in the late 1970s and early 1980s [*Squire and Moore*, 1980; *Squire et al.*, 1983; *Wadhams et al.*, 1988]. More recently, a set of experiments were carried out using an AUV in the western Bellingshausen Sea. A detailed description of these experiments can be found in *Hayes et al.* [2007]. Note that the AUV data are based on ice conditions with small floe lengths and high ice concentrations, where we do not expect our model to perform well. Nevertheless, to understand the limits of our model, we also make comparisons between this data set and our model.

4.2. SPRI Data Collection

[25] During the SPRI experiments, a helicopter was used to visit floes at intervals along the major axis of the incoming wave spectrum. At each site, a wave buoy was inserted between floes to measure the local wave spectrum, while the flexural, heave, and surge responses of the experimental floe was measured with accelerometers and strainmeters. A mean thickness of the floes was determined by coring at each of the experimental floes. Floe size distributions along the flight path into the ice were derived from overlapping vertical photography from a helicopter. The main sources of experimental error were changes in the swell conditions during the experiment, difficulties in determining the ice floe size distribution and thickness, and differences in the swell direction for different periods or multidirectional swell.

[26] From *Wadhams et al.* [1988], we have the attenuation coefficients derived from experiments in the Greenland Sea in September 1978, September 1979, and July 1983. We

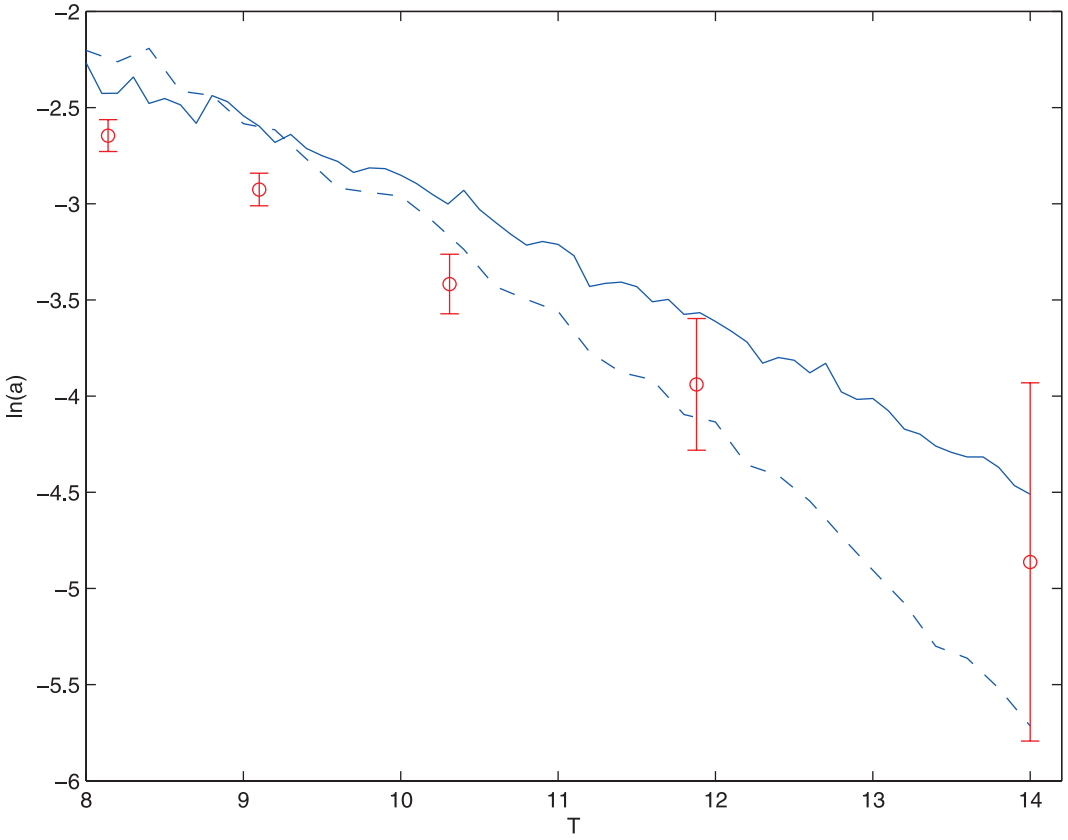

Figure 9. The attenuation coefficients for our model with mean floe length 1000 m (solid line) and mean floe length 100 m (dashed line) from the model and the measurements from the Greenland Sea experiment on 4 September 1979 (o), against *T*. Error bars are included on the experimental data points.

also have the attenuation coefficients from the Bering Sea in March 1979 and February 1983. Unfortunately accurate attenuation coefficients could not be calculated from the Greenland Sea in 1978 due to possible reflection or absorption of waves from the fjords. We also do not compare against the Bering Sea 1979 experiment, as the attenuation coefficient from the experimental data unexpectedly increases for long periods. We suspect the increase may be due to an experimental error.

4.2.1. 1979 Greenland Sea

[27] In 1979, two experiments were made in the King Oscars Fjord area of east Greenland [*Wadhams*, 1979]. During the first experiment on 4 September, the region consisted of a reasonably uniform 30% cover of multiyear floes of typical diameter 50–80 m. We model for an ice concentration of 0.3 and for floe lengths of both 50 and 80 m. On 10 September, the ice cover was more sparse and the floes were generally larger. We estimate $L = 80$ m with an ice concentration of 0.17. Ice thicknesses could not be determined on both the 4th and 10th of September, and we have resorted to taking the floe thickness from the 1978 data which, based on 14 measurements through smooth areas, gave 3.1 m (a tenuous assumption but we have no better method). It is worth noting that *Overgaard et al.* [1983] suggested this value was an underestimate of the true mean thickness, but as we have no way of verifying this we select τ distributed about 3.1 m with a relatively large standard deviation of 0.4. We expect these two experiments will provide the best fit in comparison to our model, as the ice conditions at the time of the experiments consisted of low concentration and large floe length.

4.2.2. 1983 Bering Sea

[28] During 1983, as part of the MIZEX West study, two experiments took place on 7 February in the Bering Sea [*Wadhams et al.*, 1988]. For each of the experiments, the floe thicknesses were estimated to be distributed with 20% 0.4 m floes, 40% 0.7 m floes, and 10% 1.7 m floes (the addition to 70% is from [*Wadhams et al.*, 1988]). We select τ such that it is distributed about 0.7 m with a standard deviation of 0.4 m. *Perrie and Hu* [1996] compare their model to the Bering Sea 7 February 1983 data, where they assume that the floe diameter is 14.5 m. We therefore set $L = 14.5$. Note that *Perrie and Hu* [1996] select a mean floe thickness of 1.5 m. On 7 February, the total floe concentration in the segments analyzed was 59–86%, so we estimate ice concentration is 0.72. For this experiment, we expect our model to provide a poorer fit due to the higher ice concentrations and shorter average floe lengths.

4.3. AUV Data

[29] These experiments are described in detail in *Hayes et al.* [2007]. An upward looking ADCP was mounted on an AUV. AUVs have advantages over accelerometer packages in that they sample all surface types, not just open water or sufficiently large floes; they sample at high resolution; they sample a large portion of the MIZ over short timescales; and

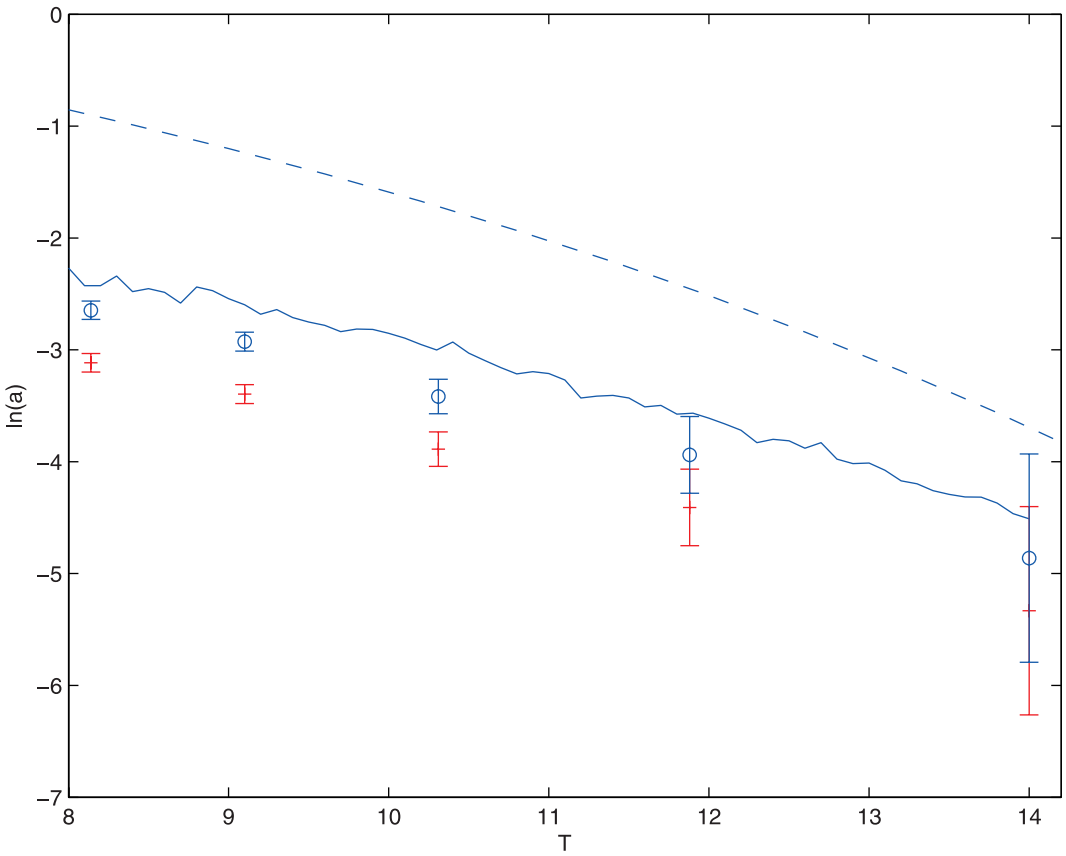

Figure 10. The attenuation coefficients against T for our model (solid line) and for Wadhams' attenuation theory given by (12), where T_3 is given by T_{av} (dashed line). The Greenland Sea experiment on 4 September 1979 is also plotted for L = 50 (+) and L = 80 (o). Error bars are included on the experimental data points.

they are remote platforms, so that they are not affected by wave motion. The Autosub AUV completed four experiments west of the Antarctic Peninsula in the Bellinghausen Sea during 22–25 March 2003. For some experiments, a mean current caused the sub to drift so that its line of travel was not necessarily along the direction of the swell nor at right angles to the ice edge. A thorough study of the ice conditions at the time of the experiments was not conducted; estimations from the ship were made for each experiment. *Hayes et al.* [2007] notes that the attenuation coefficients for waves of period longer than 16 s might be compromised by possible surge response of the vehicle.

[30] On 25 March, experiment 324 sampled roughly 10 km^2 of sea ice and traversed the ice edge twice (on entering and exiting). Ice conditions were recorded from four locations from the ship several kilometers into the ice. The sea ice was reported to consist of 100% ice coverage, 20% brash and 80% multiyear or first-year ice of thickness 1.5–2 m. We therefore select ice concentration to be 1 and τ to be normally distributed with mean 1.75 m and standard deviation of 0.5 m. Floe diameter was recorded to be less than 20 m, we select L = 20. Mission 323 took place on 24 March. Here ice coverage was again 100%; 60% first-year ice floes with diameter less than 20 m and 0.5–0.75 m thick and 40% was brash ice 0.5 m thick. To simulate, we select ice concentration to be 1, τ to be normally distributed with mean 0.625 and standard deviation 0.4 m, and L = 20. During the experiments, the AUV was not set up to record wave properties under both open water and under ice. Therefore, during experiment 323 on the 23 March, wave properties beyond 2 km from the ice edge were not measured due to a region of open water. Hence for this experiment no wave attenuation was recorded. Finally, for experiment 321 on 22 March, the region was completely under ice at 100 m depth and again no records were made. We do not expect our model to perform well against this data because the ice coverage is very high and floe lengths are small, but comparison serves a useful guide to establish a range of validity for our model.

5. Comparison of Model and Experiment

[31] We compare the energy attenuation coefficients calculated from the SPRI and AUV experimental data against our model and the approximation theories. It would be beneficial to also compare our data to the LIMEX dat set *Liu et al.* [1991], but unfortunately we have been unable to obtain this data. The energy attenuation coefficients, α, provided in *Wadhams et al.* [1988] and *Hayes et al.* [2007], are calculated by fitting an exponential curve of E versus distance from the ice edge. Our energy attenuation coefficients, a, are per floe number ($\Lambda = xC/L$ where L is the average length of the floes and C is the floe concentration). Therefore $\alpha = aC/L$.

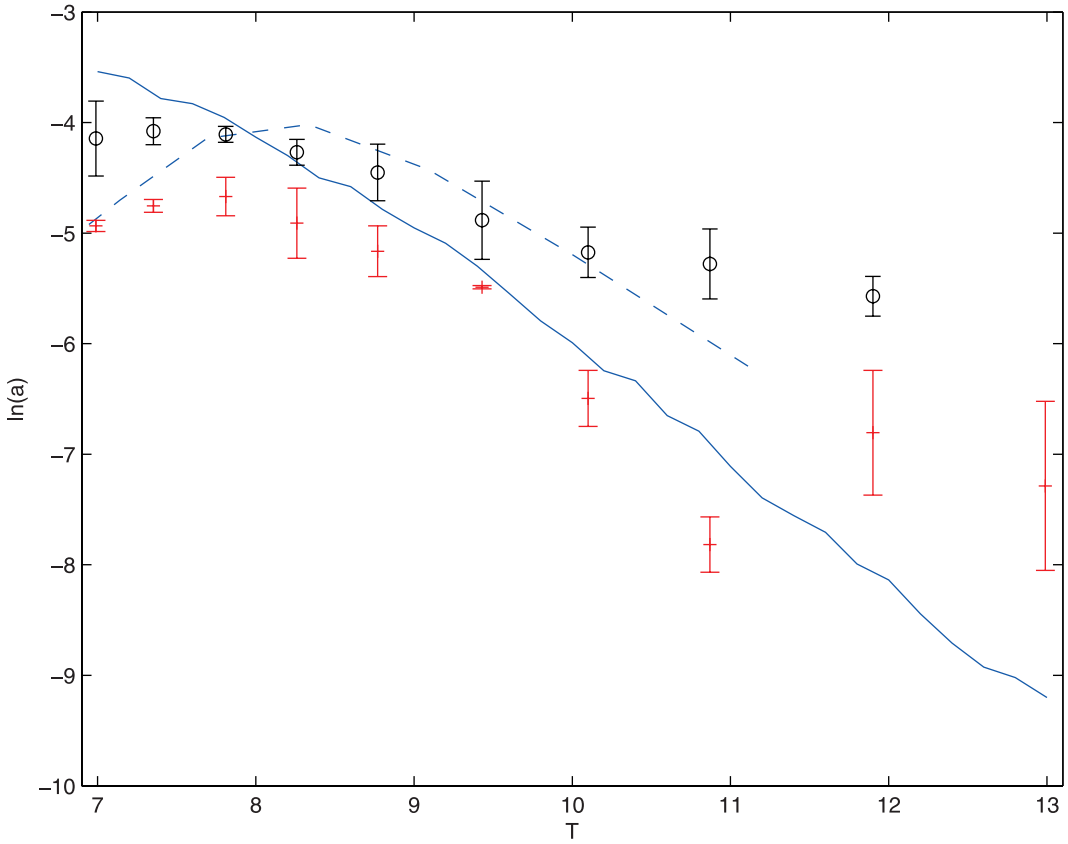

Figure 11. Our model (solid line) and the model of *Perrie and Hu* [1996] (dashed line) compare with the two Bering Sea experiments on 7 February 1983. Error bars are included on the experimental data points.

[32] We present the Greenland Sea data from 10 September 1979 in Table 1 and Figure 8. Generally the data and model are in good agreement. They slightly disagree for small periods where a rollover (a trend of decreasing attenuation as the period becomes smaller) occurs in the field data, and for longer periods where our model slightly under-predicts the attenuation coefficients. We plot the experimental data with error bars, the predicted value from our model as a solid line and its 95% confidence interval as dotted lines. We also plot *Wadhams et al.* [1986]'s approximation theory given by equation (12) as a dashed line. This clearly shows that the approximation theories are over predicting the attenuation coefficient. Interestingly, the results in *Wadhams et al.* [1988] agree with the experimental data better than the approximate theory presented here does. This might be due to the error in their solution for the single floe scattering producing lower attenuation coefficients than are obtained with the correct single floe scattering as presented here. It is also worth mentioning that there is a range in the data and in other situations the approximate theory may perform better.

[33] Figure 9 is a similar plot but is for the 4th of September Greenland Sea 1979. In this case, our model slightly over predicts the attenuation coefficient. We calculate the attenuation coefficient using our long floe assumption ($L = 1000$ m, solid line), and we also run the simulation using a value for the floe length closer to the real value ($L = 100$ m, dashed line). The attenuation coefficient for the measured data lies between the two values of floe length. Figure 10 shows the same measured data with two versions of the floe length (50 m and 80 m) for the experiment results. This figure shows the linear scaling of the attenuation coefficient with this property. It is clear that there is a great deal of uncertainty in any comparison of these experiments with our model, highlighting the need for better experimental results. Figure 10 also plots the approximation theory, which is again over predicting the attenuation coefficients.

[34] For the Bering Sea 1983 experiments (Figure 11) (note there were two experiments on the same day with different result, despite the conditions being almost identical), we compare our model to the model of *Perrie and Hu* [1996] (shown in the dashed line). We find the two models are in close agreement for this case of small floes. This is because our model reduces to the rigid body model in the limit of small floes. Our model approximately lies between the two experiments, and it is generally a very good representation of the experimental data. *Perrie and Hu* [1996]'s model has slightly higher attenuation coefficients, but it represents the rollover in the first experiment very well, while ours does not represent the rollover at all. Note that the mean floe thickness used in *Perrie and Hu* [1996]'s model was 1.5 m rather than 0.7 m. Interestingly, note that our model under-predicts the attenuation coefficients for periods greater than 12 s, which will be discussed shortly.

[35] We present the Autosub AUV data in Figure 12. There is little agreement with our model for these ice

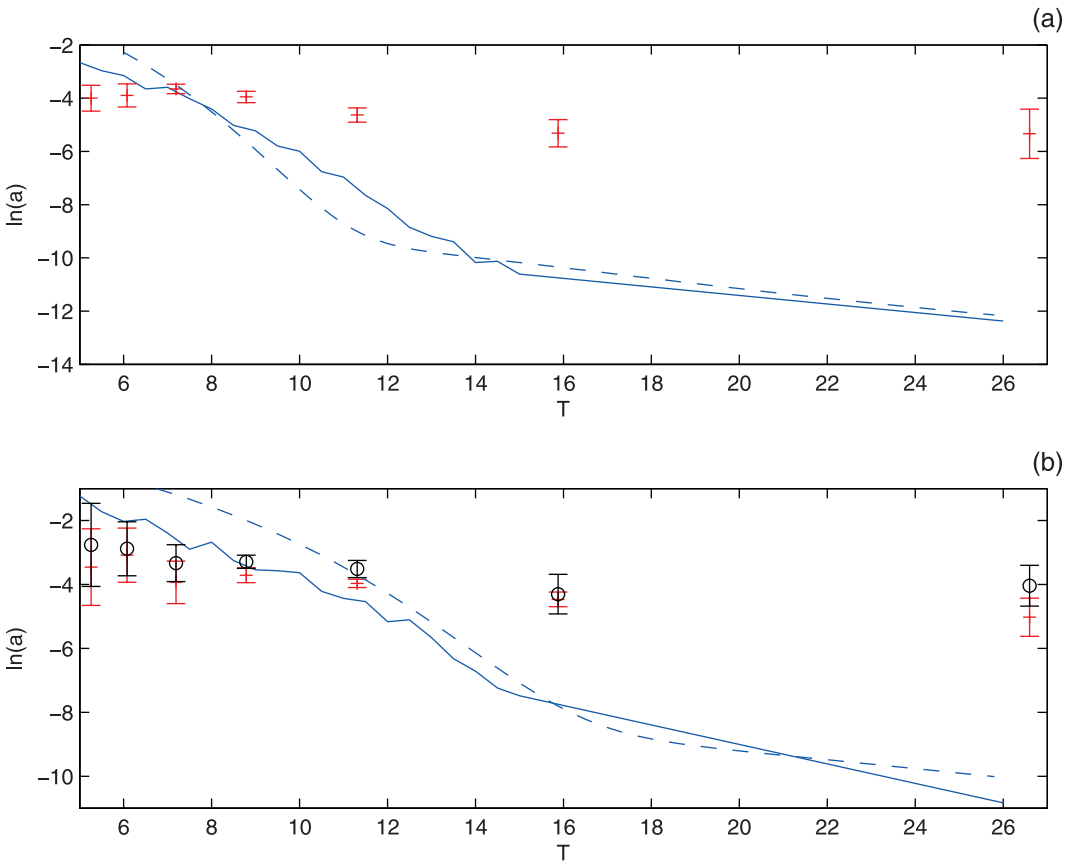

Figure 12. Comparison of our model (solid line), Wadhams' approximation theory given by (12), where T_3 is given by T_{av} (dashed line), and the Autosub AUV data. Subplot (a) is for experiment 323 and subplot (b) is for experiment 324. Error bars are included on the experimental data points.

conditions. The results for shorter periods are of similar order of magnitude, but our model is clearly under-predicting the attenuation rate for longer periods. Note, however, that there may have been errors in the experimental data for long periods, due to the possible surge response of the vehicle at long periods.

6. Modeling Ice Breaking

[36] Incoming waves cause ice floes to bend. If the bending induces sufficient strain, fracture will occur [*Squire*, 1993]. The breaking of large continuous floes and landfast ice supplies the MIZ with ice floes and determines the floe size distribution of the MIZ [*Langhorne et al.*, 1998]. During ocean wave experiments, strain gauges were fixed to the upper surface of sea ice floes in the Arctic, which provided some direct measurements of sea ice fracturing. Results from these experiments have shown an ice island to fracture at a strain of 3×10^{-5} [*Goodman et al.*, 1980] and sea ice to fracture at a strain from 4.4×10^{-5} to 8.5×10^{-5} [*Squire and Martin*, 1980]. On the basis of a series of experiments carried out in the McMurdo Sound, Antarctica, *Langhorne et al.* [1998] deduce that sea-ice fatigues when it is cyclically stressed. This fatigue can cause the ice to fracture and break up at stresses well below its flexural strength. Using these experiments, *Langhorne et al.* [2001] predict the lifetime of the sea-ice as a function of significant wave height and sea-ice brine fraction. In general, if the strain is less about 3×10^{-5}, the ice seems to have an infinite resistance to failure (personal correspondence with T. Haskell) and we take this as our value for ice breaking. Models of strain through an ice sheet combined with these experimental results can be used to predict floe breakup in a MIZ. We use our model to predict the number of floes which will be broken for a given incident wave spectrum at the ice edge. Essentially we input a given wave spectrum and calculate the number of floes which are required to reduce the wave height below a height which is considered minimal to induce floe breaking. This is equivalent to allowing the incident waves to break the ice and recalculating the spectrum until we find that no further breaking will occur.

6.1. Strain

[37] We assume we have small-amplitude waves ($\frac{\partial \eta^2}{\partial x} \ll 1$). The strain, S, at the surface of the ice due to an incident wave is therefore

$$S(x) = \frac{\tau}{2} \frac{\partial^2 \eta(x)}{\partial x^2} \tag{14}$$

where η is the displacement. S is easily derived from our expression for the velocity potential (8).

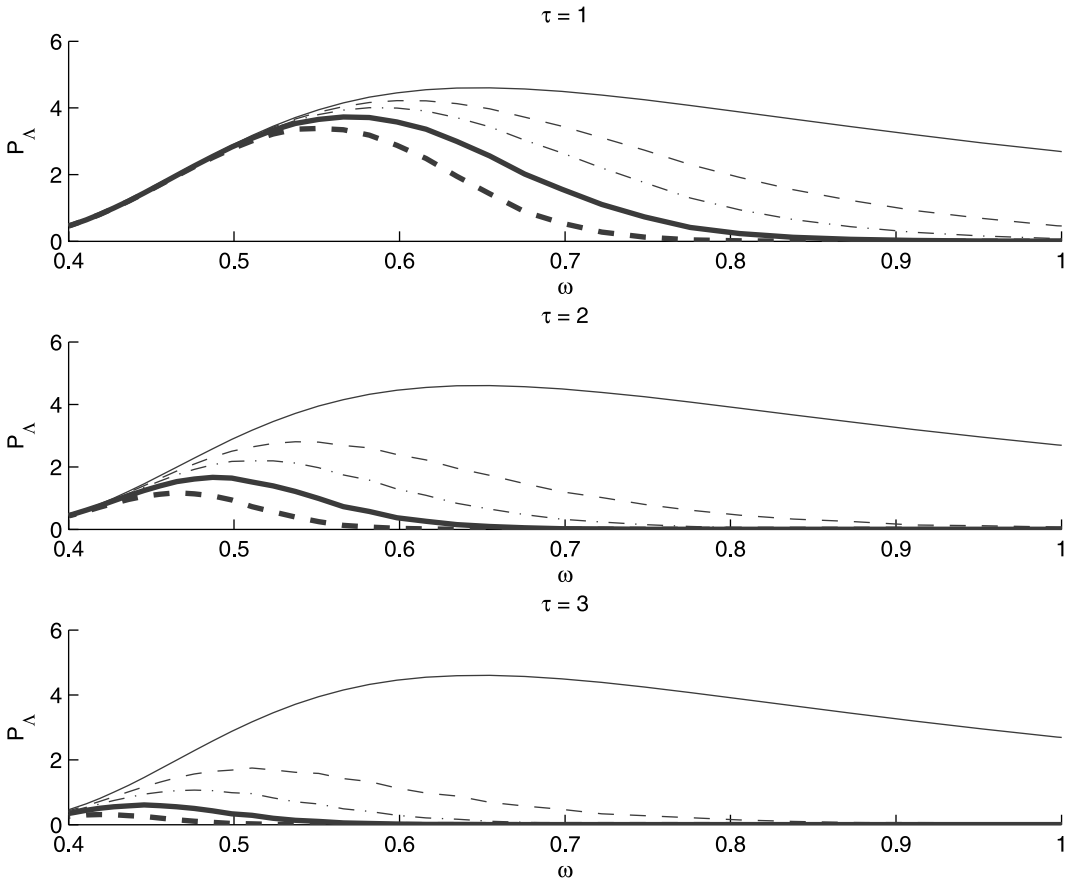

Figure 13. The spectrum of P_Λ after 0 floes (-), 25 floes (−), 50 floes (..), 100 floes (-.-), and 200 floes (-) for τ = 1, 2, and 3 as shown. ω is the frequency in Hertz.

6.2. The Strain for a Wave Spectrum

[38] We assume that the incident wave energy is given by the Pierson–Moskowitz spectrum [*Pierson and Moskowitz*, 1964] given by:

$$P(\omega) = \zeta g^2 (2\pi)\omega^{-5} e^{\frac{5}{4}\left(\frac{\omega_m}{\omega}\right)4} \tag{15}$$

where ω_m is the peak frequency and ζ is Phillip's constant which is found experimentally to be approximately 1.2×10^{-2} [*Phillips*, 1977].

[39] As the wave propagates through the ice, the wave spectrum will be altered due to dampening caused by the ice. If we can estimate the attenuation of the wave energy, we can estimate the change in the wave spectrum for a given τ and Λ so that

$$P_\Lambda(\omega) = P(\omega)e^{-a(\omega)\Lambda} \tag{16}$$

where the attenuation coefficients $a(\omega)$ are given by our model. We calculate the strain using the strain envelope given by

$$S_E(x) = \sqrt{\int_0^\infty |P_\Lambda(\omega)S(x,\omega)|^2 d\omega} \tag{17}$$

[*Fox and Squire*, 1991]. Note that the strain envelope is a function of x and we will consider the maximum value.

[40] Figure 13 shows the change in the wave spectrum with number of ice floes for a peak period of 10 s ($\omega_m = 2\pi/10$). This figure shows that there is a strong attenuation of high-frequency waves, and that as the thickness is increased the cut off frequency below which there is little attenuation decreases. It is important to note that there is virtually no attenuation of the high-frequency (long-period) waves from our scattering model.

[41] Figure 14 shows the maximum of the strain envelope as a function of number of floes for various floe thicknesses, for an incident spectrum with peak period 10 s. Also shown is the strain 3×10^{-5}, below which experiments have shown that floe breaking no longer occurs. This figure implies that, for this incident wave spectrum, floe breaking will occur almost indefinitely for small floe thickness. This seems anomalous, and it implies that our model is failing to correctly estimate the attenuation coefficient for long period waves, or that the floe breaking strain is incorrectly estimated. We believe that the former is more likely due to the very small attenuation of the long period waves, and we conclude that there is an underestimation of attenuation coefficients for long periods from our scattering model. Note that, even if we use the approximate theories for the

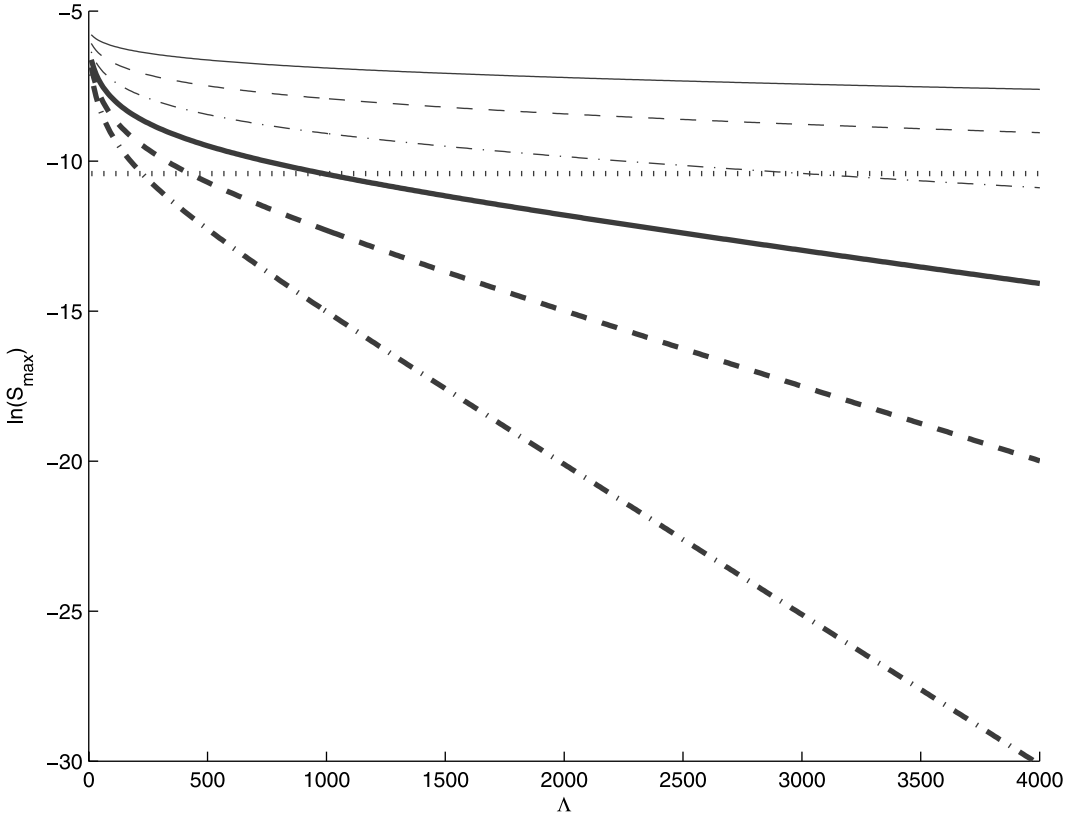

Figure 14. The natural logarithm of the maximum of the strain envelope versus Λ for $\tau = 1$ m (-), $\tau = 1.5$ m (–), $\tau = 2$ m (-.-), $\tau = 2.5$ m (-), $\tau = 3$ m (–), and $\tau = 3.5$ m (-.-). The line 3×10^{-5} (..) above which floe breaking occurs is also plotted.

scattering, we find that there is still an underestimation of the attenuation coefficients for long periods (Figure 12).

7. Summary

[42] We have presented a model for predicting wave attenuation in the MIZ, based on a solution for wave propagation under two-dimensional floating elastic plates. The only physics in our model is due to the effect of an elastic plate on the water surface and we have neglected all nonlinear effects as well as floe collisions and viscosity. Our model predicts the exponential decay of wave energy with distance of propagation through the MIZ, once resonance effects have been removed by averaging over a distribution of floe lengths. We found that the attenuation coefficient, provided the floes are sufficiently large, is a function of number of floes and is independent of average floe length. Our results have been summarized in a graph of attenuation coefficient as a function of period for various floe thicknesses. We have compared our model against a series of field experiments carried out in the Arctic seas by the SPRI and against a set of experiments carried out off the West Antarctic Peninsula.

[43] We found successful agreement between the model and the experimental data for the experiments most applicable to our model. Surprisingly we found that generally, even for the experiments less applicable to our model, there is some agreement between our model and the experimental data for short periods. However, as the ice concentration increases and floe length decreases, the under-prediction of the attenuation coefficient increases and this is especially apparent at long periods. This under-prediction may be accounted for by the fact that our scatter model is restricted to floe lengths which are generally large. As the pack becomes closer, the floes can no longer surge in response to the waves, and hence wave attenuation may be occurring more significantly in the form of viscous losses from the boundary layer under the ice rather than from losses due to scattering [*Squire et al.*, 1995]. Increased wave attenuation may also be a result of energy loss due to the inelasticity of sea ice. However the cause of the attenuation at long periods remains an open question. We conclude that for small floe sizes and high ice concentrations, wave attenuation is not primarily due to wave scattering. A scattering model, however, is generally a good approximation for the attenuation coefficient of short period waves. We also conclude that a scattering model is a good overall approximation for ice conditions consisting of large floe lengths and a small ice concentration and hence minimal floe collisions. We find that the decay rates of the model generally agree well with the field experiments, provided that the floe lengths are sufficiently large and the concentration is not too high. Note that we had a small data set, where the variables L, τ, and C were only rough estimates of the floe characteristics at the time of the experiments. Further experiments are required to make proper comparison with our model and to accurately determine its range of validity.

[44] We also present a model for predicting the strain and floe breaking using our attenuation model. The results from this strongly suggest that our model cannot account for the attenuation coefficient at long periods.

Appendix A: Approximation Theory

[45] We derive here an approximate scattering theory based on the semi-infinite solution with water on one side and a plate on the other, which gives the solution for a single finite floe. The theory for this was given in *Meylan and Squire* [1993]. This is the semi-infinite problem in our formulation with $\Lambda = 2$, and also the problem which was solved by *Fox and Squire* [1994]. We denote by T_{wp} and R_{wp}, the transmitted and reflected energy from a semi-infinite body of water to a semi-infinite plate. If we assume that a plate is large enough so the damped and evanescent waves diminish by the time they reach the edge of the plate, we can find R_1 and T_3 for the finite plate. The transmitted and reflected coefficients of a wave traveling from a semi-infinite plate to a semi-infinite body of water, denoted by T_{pw} and R_{pw}, can be expressed in terms of T_{wp} and R_{wp} as

$$T_{pw} = \frac{1 - |R_{wp}|}{T^*_{wp}}, R_{pw} = -\frac{R^*_{wp} T_{wp}}{T^*_{wp}} \tag{A1}$$

[*Meylan and Squire*, 1993]. We now consider the problem of a long and wide finite plate surrounded by water and obtain

$$R_1 = R_{wp} - \frac{R^*_{wp} T^2_{wp} \left(1 - |R_{wp}|\right) e^{2k_2(1)(l-r)}}{T^{*2}_{wp} - R^{*2}_{wp} T^2_{wp} e^{2k_2(1)(l-r)}},$$
$$T_3 = \frac{|T_{wp}|^2 \left(1 - |R_{wp}|\right) e^{k_2(1)(l-r)}}{T^{*2}_{wp} - R^{*2}_{wp} T^2_{wp} e^{2k_2(1)(l-r)}}. \tag{A2}$$

Since, T_3 in equation (A2) is periodic in floe length, we can calculate the average of $|T_3|^2$ over one period, i.e.,

$$|T_{av}|^2 = \frac{1}{2\pi} \int_0^{2\pi} \frac{|T_{wp} T_{pw}|^2}{1 - |R_{wp}|^2} dt \tag{A3}$$

[*Williams*, 2005] to obtain

$$|T_{av}|^2 = \frac{|T_{wp} T_{pw}|^2}{1 - |R_{wp}|^2}. \tag{A4}$$

[46] **Acknowledgments.** This research was supported by Marsden grant UOO308 from the New Zealand government. The numerical code to solve the dispersion equations was provided by Tim Williams. We would also like to thank Daniel Hayes for supplying the AUV experiment results and the referees for their feedback.

References

Dean, C. H. (1966), The attenuation of ocean waves near the open ocean/pack ice boundary, in *Symposium on Antarctic Oceanography*, pp. 13–16, Scientific Committee on Antarctic Research, Santiago, Chile.

Dixon, T. W., and V. A. Squire (2001), Energy transport in the marginal ice zone, *J. Geophys. Res.*, *106*(C9), 19,917–19,927.

Fox, C., and V. A. Squire (1991), Strain in shore fast ice due to incoming ocean waves and swell, *J. Geophys. Res.*, *96*(C3), 4531–4547.

Fox, C., and V. A. Squire (1994), On the oblique reflexion and transmission of ocean waves at shore fast sea ice, *Philos. Trans. R. Soc.*, *A 347*(1682), 185–218.

Goodman, D. J., P. Wadhams, and V. A. Squire (1980), The flexural response of a tabular ice island to ocean swell, *Ann. Glaciol.*, *1*, 23–27.

Hayes, D. R., A. Jenkins, and S. McPhail (2007), Autonomous underwater vehicle measurements of surface wave decay and directional spectra in the marginal ice zone, *J. Phys. Oceanogr.*, *37*(1), 71–83.

Isaacson, M. (1982), Fixed and floating axisymmetric structures in waves, *J. Waterw. Port Coastal Ocean Div. Am. Soc. Civ. Eng.*, *108*(2), 180–199.

Kohout, A., and M. H. Meylan (2006), A model for wave scattering in the marginal ice zone based on a two-dimensional floating elastic plate solution, *Ann. Glaciol.*, *44*, 101–107.

Kohout, A., M. H. Meylan, S. Sakai, K. Hanai, P. Leman, and D. Brossard (2007), Linear water wave propagation through multiple floating elastic plates of variable properties, *J. Fluids Struct.*, *23*(4), 649–663.

Langhorne, P. J., V. A. Squire, C. Fox, and T. G. Haskell (1998), Break-up of sea ice by ocean waves, *Ann. Glaciol.*, *27*, 438–442.

Langhorne, P. J., V. A. Squire, C. Fox, and T. G. Haskell (2001), Lifetime estimation for a land-fast ice sheet subjected to ocean swell, *Ann. Glaciol.*, *33*, 333–338.

Linton, C. M., and P. McIver (2001), *Handbook of Mathematical Techniques for Wave/Structure Interactions*, 304 pp., Chapman and Hall/CRC, Boca Raton, Fla.

Liu, A. K., B. Holt, and P. W. Vachon (1991), Wave propagation in the marginal ice zone: Model predictions and comparisons with buoy and synthetic aperture radar data, *J. Geophys. Res.*, *96*(C3), 4605–4621.

Masson, D., and P. LeBlond (1989), Spectral evolution of wind-generated surface gravity waves in a dispersed ice field, *J. Fluid Mech.*, *202*, 111–136.

Meylan, M. H. (2002), The wave response of ice floes of arbitrary geometry, *J. Geophys. Res.*, *107*(C6), 3005, doi:10.1029/2000JC000713.

Meylan, M. H., and D. Masson (2006), A linear Boltzmann equation to model wave scattering in the marginal ice zone, *Ocean Modell.*, *11*(3–4), 417–427.

Meylan, M. H., and V. A. Squire (1993), Finite floe reflection and transmission coefficients from a semi-infinite model, *J. Geophys. Res.*, *98*(C7), 12,537–12,542.

Meylan, M. H., and V. A. Squire (1994), The response of ice floes to ocean waves, *J. Geophys. Res.*, *99*(C1), 891–900.

Meylan, M. H., V. A. Squire, and C. Fox (1997), Towards realism in modeling ocean wave behavior in marginal ice zones, *J. Geophys. Res.*, *102*(C10), 22,981–22,991.

Overgaard, S., P. Wadhams, and M. Lepparanta (1983), Ice properties in the Greenland and Barents seas during summer, *J. Glaciol.*, *29*(101), 142–164.

Perrie, W., and Y. Hu (1996), Air–ice–ocean momentum exchange. Part 1: Energy transfer between waves and ice floes, *J. Phys. Oceanogr.*, *26*, 1705–1720.

Phillips, O. M. (1977), *The Dynamics of the Upper Ocean*, 2nd ed., Cambridge Univ. Press, New York.

Pierson, W. J., and L. Moskowitz (1964), A proposed spectral form for full-developed wind sea based on the similarity law of S. A. Kitaigorodoskii, *J. Geophys. Res.*, *69*, 5202.

Robin, G. Q. (1963), Wave propagation through fields of pack ice, *Philos. Trans. R. Soc.*, *S-A 255*(1057), 313–339.

Sakai, S., and K. Hanai (2002), Empirical formula of dispersion relation of waves in sea ice, in *Ice in the Environment: Proceedings of the 16th IAHR International Symposium on Ice*, pp. 327–335.

Squire, V., and S. C. Moore (1980), Direct measurement of the attenuation of ocean waves by pack ice, *Nature*, *283*(5745), 365–368.

Squire, V., P. Wadhams, A. M. Cowan, S. O'Farrell, and R. Weintraub (1983), MIZEX 83 data summary, *SPRI Technical Report 83-1*, Scott Polar Research Institution.

Squire, V. A. (1993), The breakup of shore-fast sea ice, *Cold Reg. Sci. Technol.*, *21*, 211–218.

Squire, V. A., and S. Martin (1980), A field study of the physical properties, response to swell, and subsequent fracture of a single ice floe in the winter Bering sea, *Univ. Wash. Sci. Rep. 18*, Dept. Atmos. Sci. and Oceanogr.

Squire, V. A., J. P. Dugan, P. Wadhams, P. J. Rottier, and A. J. Liu (1995), Of ocean waves and sea ice, *Annu. Rev. Fluid Mech.*, *27*, 115–168.

Wadhams, P. (1975), Airborne laser profiling of swell in an open ice field, *J. Geophys. Res.*, *80*, 4520–4528.

Wadhams, P. (1978), Wave decay in the marginal ice zone measured from submarine, *Deep-Sea Res.*, *25*, 23–40.

Wadhams, P. (1979), Field experiments on wave–ice interaction in the Labrador and East Greenland currents, 1978, *Polar Rec.*, *19*(121), 373–379.

Wadhams, P. (1986), The seasonal ice zone, in *The Geophysics of Sea Ice*, edited by N. Untersteiner, pp. 825–991, Plenum, New York.
Wadhams, P. (2000), *Ice in the Ocean*, Gordon and Breach Science.
Wadhams, P., V. A. Squire, J. A. Ewing, and R. W. Pascal (1986), The effect of marginal ice zone on the directional wave spectrum of the ocean, *J. Phys. Oceanogr.*, *16*, 358–376.
Wadhams, P., V. A. Squire, D. J. Goodman, A. M. Cowan, and S. C. Moore (1988), The attenuation rates of ocean waves in the marginal ice zone, *J. Geophys. Res.*, *93*(C6), 6799–6818.
Williams, T. D. (2005), Reflections on ice: The scattering of flexural-gravity waves by irregularitiies in Arctic and Antarctic ice sheets, Ph.D. thesis, Univ. of Otago, Dunedin, New Zealand.
Williams, T. D., and V. A. Squire (2004), Oblique scattering of plane flexural-gravity waves by heterogeneities in sea-ice, *Proc. R. Soc. Lond.*, *Ser-A 460*(2052), 3469–3497.
Williams, T. D., and V. A. Squire (2006), Scattering of flexural-gravity waves at the boundaries between three floating sheets with applications, *J. Fluid Mech.*, *569*, 113–140.

A. L. Kohout and M. H. Meylan, Department of Mathematics, University of Auckland, Private Bag 92019, Auckland, New Zealand. (akohout@math.auckland.ac.nz; meylan@math.auckland.ac.nz)